Calibration Properties of CHANDRA HETG Spectra Observed in CC-Mode

Norbert S. Schulz,[1] and the Chandra ACIS Calibration Team,[1],[2],[3]

1. Introduction

The ACIS detector onboard Chandra offers two read out modes, Timed Event (TE) mode and Continuous Clocking (CC) mode. In TE mode events are accumulated for a specified amount of time (frame time (ft)) and are collectively read out into a frame store buffer. After a deadtime, the next frame cycle begins. Frame times can be set up to 10 seconds, the standard time for a full frame (1024 rows) is 3.2 seconds. This time can be reduced further through the creation of subarrays by limiting the number of rows. The lowest subarray size is 128 rows which corresponds to about 350 msec of frametime. In the second mode events are read out continuously and here only the row by row readout time is effective which amounts to 2.85 sec. CC-mode is applied for various reasons, its original dedication was to offer a fast readout mode for the use of the ACIS detector.

Soon after the launch of Chandra another application of CC-mode was introduced and this refers to the mitigation of pile up in the charge coupled devices (CCDs) of the ACIS detector in bright sources. Photon intensities that exceed about 0.01 counts per pixel per frametime (cts/pix/ft) in a CCD cause events to pile up, i.e. there is a significant probability that the device cannot recognize two single photons and will register these at the sum of their energies. This probability goes fairly linear with frametime and thus can be reduced by shorter frametimes. In timed event mode this is limited to the lowest subarray size and thus 350 msec. The best possibility in high intensity cases then is the application of CC-mode which reduces pileup by a about a factor 103.

However the application of CC-mode comes at the expense of imaging as any observed frame is eventually collapsed into one row. We therefore do not find many bare ACIS observations of high intensity objects in the Chandra archive. However, CC-mode found its application in grating spectroscopy. Chandra has three grating types, low (LEG), medium (MEG), and high (HEG) energy gratings for high resolution spectroscopy in the bandpass

[1]Kavli Institute for Astrophysics and Space Research, Massachusetts Institute of Technology, Cambridge, MA 02139.

[2]Center for Astrophysics, Cambridge, MA 02139.

[3]Marshall Space Flight Center, Huntsville, AL.

from 0.1 to 8 keV at up to 1200 in spectral resolving power. The MEG and HEG gratings are mounted on the high energy transmission grating (HETG) rack and produce an X-ray image in their zeroth order and disperse point sources into two different grating spectra which are simultaneously captured by the ACIS-S array. The array contains six CCD devices labeled from S0 to S5 with the zeroth order image on S3. The HETG itself also acts as a blocking devise for 0th order events because the grating facets are mounted on a μ m thick polyimid film, which reduces flux be another factor of a about four and a half.

The dispersive property of the grating allows to record proper X-ray spectra with source intensities of up to several tens of mCrab with the MEG and HEG using reduced frametimes through subarrays in TE-mode. Many bright Galactic plane and bulge sources and X-rays transients reach much higher fluxes and pileup in grating spectra becomes a problem. Once the rate in pixels recording the dispersed photons exceeds the pileup limit, photons get redistributed from the 1st order into the higher orders. Even though advanced algorithms can fully repair continuum spectra under various circumstances, it is impossible to treat discrete line features, specifically emission lines. Here spectra in CC-mode are specifically useful as they remain pileup-free for basically all existing X-ray fluxes and thus preserve exisiting line features. This, however, comes at the price that continuum information gets lost and/or our ability to calibrate and analyse broadband continua becomes highly limited.

In the following we decribe fundamental properties of bright CC-mode X-ray spectra using the HETG and the ACIS-S detector array. Some emphasis is given on setting flux guidelines of when to use CC-mode. specific properties of spectra as a consequence of collapsing the dispersed image, calibration deficiencies, and configuration guidelines for future observations.

2. Calibration Sources

Most data sets used for this study come from the guest observer observation program or are guaranteed time observations. In some cases we added a calibration follow-up observation in order to compare results from the uses of a different configuration or instrument setting. Table 1 lists some relevant properties of X-ray sources and instrument configurations. 4U1957+115 is one of the sources we observed in the calibration program in three parts consisting of a TE mode, CC-mode, and TE-mode in direct succession. It is the faintest of all sources but with 35 mCrab is just bright enough to allow TE mode observations with only little pile-up.

TABLE 1 CALIBRATION SOURCE PROPERTIES

Sources	Obsids	Flux (1)	Flux (2)	N_H (3)	exposure (4)	Mode	Subarray	Z-Sim (5)
4U 1957+115	10659	35	0.80	0.15	10	TE	15, 440	-6.8
	10660		0.80	0.15	20	CC	–	-6.8
	10661		0.80	0.15	10	TE	15, 440	-6.8
4U 1728-34	2748	85	2.00	2,51	30	TE	1, 400	-7.49
	6567		2.00	2,51	160	CC	–	-4.0
GX 13+1	11817	330	7.94	3.16	30	TE	1, 350	-8.0
	11818		7.94	3.16	30	CC	faint	-8.0
	13197		7.94	3.16	10	CC	graded	-8.0
GX 349+2	12199	660	15.8	1.99	20	CC	–	-6.14
	13220		15.8	1.99	20	TE	1, 300	-11.3
	13221		15.8	1.99	40	CC	–	-6.14
Cyg X-2	8170	540	13.2	0.32	70	CC	–	-6.14
	8599		13.2	0.32	70	CC	–	-6.14
	10881	340	8.2	0.32	100	CC	–	-6.14
GX 5-1	5888	700	17.0	3.36	50	CC	–	-11.3

(1) [mCrab], (2) [10^9erg cm^{-2} s^{-1}], (3) [10^{22} cm^{-2}], (4) [ks], (5) [cm]

Figure 1 shows images of the dispersed spectra on the ACIS-S array in TE mode. In CC mode there are no full images as the y-pixel scale is collapsed. The top panel shows 4U 1957-115 observed in a custom 440 row subarray mode allowing for observing most all of the source relevant HETG bandpass. The middle panel shows the bright source GX 13+1 observed with a more restricted 350 row subarray and a more limited bandpass to about 18 Å. The lower panel shows the even brighter source GX 349+2 in an even more restricted subarray but now with MEG -1st and HEG +1st orders out of the array. This further reduces HETG pileup but allows a much wider bandpass at the expense of effective area and thus exposure.

The question of when and how to use TE and CC-mode to obtain HETG spectra depends on instrumental settings and basic properties of the expected spectrum. The dominating parameter is the incident source flux as it, sometimes in conjunction with photoelectric X-ray absorption, defines the choice of instrument settings. There are three main regimes to consider, which simply refer to low, medium, and high X-ray fluxes. These regimes have substantial overlaps which again depend on the choice of settings and spectral band pass.

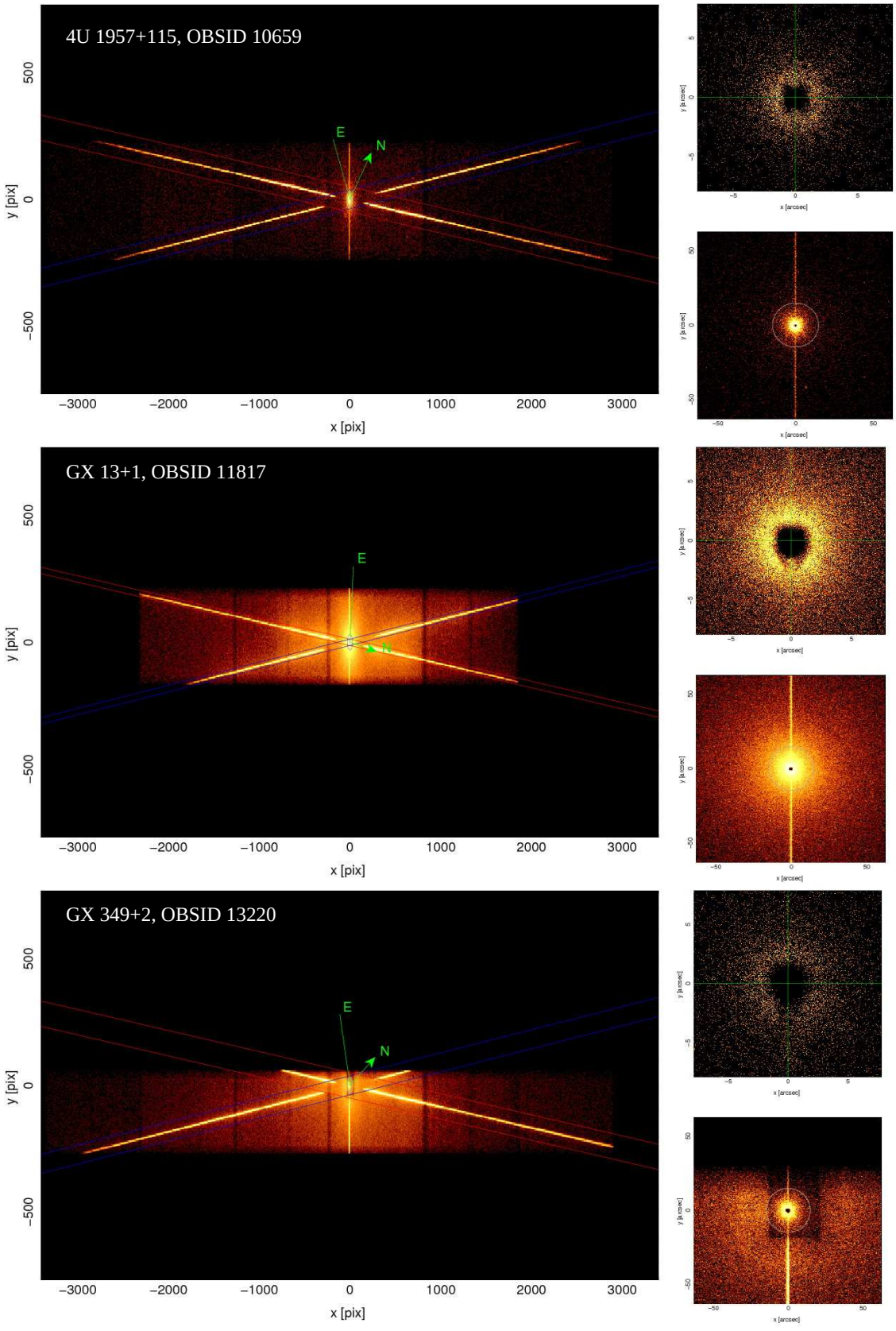

Fig. 1.— Three calibration sources observed in TE mode at different fluxes and configurations (see Table 1). The top shows the full dispersed image of obsid 10659 at a low flux. The two panels to the right show two zooms of the zero order image, which in this case indicates

2.1. Low Flux Regime (< 35 mCrab)

We consider anything that can be safely observed in TE mode without the application of restrictive subarrays part of the low flux regime. Here fluxes up to about 10 mCrab can be accomodated without pileup losses. However, as a standard mode for non-stellar fields, usually a 512 row subarray starting at the readout row is applied. This allows for about 25 mCrab without pileup losses. About 35 mCrab may be possible by restricting the bandpass through shutting off devices, though in these cases different choices of subarrays are likely more effective. We have one calibration source in the low flux regime at about 35 mCrab, 4U 1957+115, which was observed in direct succession for 10 ks in TE mode, 20 ks in CC mode, the again 10 ks in TE mode in order to exclude possible spectral variations between the TE and CC mode observations. We applied a 440 row subarray in TE mode wich allowed for some pile-up ($< 6\%$) to affect the spectra.

2.2. Medium Flux Regime (< 350 mCrab)

In general the application of subarrays can accommodate up to about 350 mCrab, but with very restrictive bandpasses and the loss of effective area but manageable pile-up losses. In the most extreme case bandpasses can be limited to > 2 keV (1.9 Å), which corresponds to a 128 row subarray at the readout row and the operation of only two devices in the array. For practical reasons it is assumed that CC-mode is only used when deemed necessary and otherwise TE mode is always desired.

Table 1 contains two calibration sources in the medium regime: 4U 1728-34 at 85 mCrab, which has been observed in TE mode with a 400 row subarray for 30 ks, but also in CC-mode for 160 ks; GX 13+1 was observed several times since launch, here we chose two GTO observations, one in TE mode with a 350 row subarray, another one with the same SIM-Z setting in CC-mode. Another 10 ks calibration observation was added to verify the use of graded mode in CC-mode. Even though CC-mode spectra are calibrated as TE mode spectra, these calibrations have to be validated.

Note, the choice of TE versus CC mode also depends on the source spectrum. The reason why GX 13+1, which at 330 mCrab is already extremely bright, could be observed in TE mode with only minor pileup losses ($< 10\%$) was because of its high X-ray absorption and relative hard spectral properties.

2.3. High Flux Regime (> 350 mCrab)

Most bright Galactic bulge sources, BH transients, some presistent LMXBs and HMXBs fall in to the high flux regime above 300 mCrab. Here in 95% of the cases it is strongly advised to use CC mode in order to preserve absorption and emission lines. However, there are many issues associated with the use of CC mode which are discussed in the following.

3. ACIS Calibration between TE and CC mode

In this section it is assumed that spectra in TE mode are sufficiently calibrated and are then used as a standard to compare with CC mode spectra. There are several issues we consider for calibration of the ACIS instrument. These are energy scale and gain, the ACIS response function, trailing charges from charge transfer inefficieny (CTI), and quantum efficieny and its uniformity. In the following we decribe possible differences between TE and CC mode and its impact on the overall ACIS calibration in CC mode.

3.1. Energy Scale and Gain

The energy (wavelength) scale in HETG spectra is defined by the dispersion equation and primarily does not depend on the ACIS PHA's other than for the moment of order sorting. It is relevant for event extraction of the spectra. The event extraction relies on the order sporting table (OSIP) which is a combination of spatial and pulse height extraction windows (see also Section "CTI Corrections"). Therefore in order to investigate differences between the behavior in TE and CC mode we look at the relative positions of the orders in pulse height (pha) space.

Figure 2 shows a slice in pha space of HETG spectral orders. In this case the pha's at 9.8±0,3 Å are shown for the MEG +1st and HEG -1st orders in three different configurations. The bright source GX 349+2 was observed in TE and CC mode in various configurations. It is bright enough to produce usable orders up to the 4th order. Anything higher likely stems from ACIS high energy CC-mode background in the OSIP extraction windows (see Sect. "CC-Mode Background"). The top and middle two panels show extractions from CC-mode configurations, the bottom two panels a TE mode observation of GX 349+2 with two grating arms located off the array. This allows to directly compare TE and CC-mode results on energy scale and gain. The statistcs of the first order peaks allow a gain determination to $< 0.5\%$, close to the 0.3% standard from the external calibration source determinations. The higher orders are fainter and here we settle for up to 3.0%, which is still well sufficient

for order sorting.

We determined first and higher order peaks at several wavelengths ranging from 2 to 18 Å for all orders where available. The PHA ratios of first to third order peak positions showed variations of less than 1.0%, ratios with and within the other orders showed variations less than 2.5%. There was no difference between CC and TE mode. This shows that the energy scale in CC mode is not significantly different to the ones used in TE mode.

The same procedure was repeated on the MEG -1st and HEG +1st orders with some different results. While the ratios with the higher orders remained within the 3% accuracy of the measurement, the first order gain determinations were only good within 3 - 5%. While this is still not problematic with respect to order sorting, it shows that there is an issue with CTI (see Sect. CTI Correction).

3.2. ACIS Response Function

In each ACIS device the response varies with increasing row numbers mainly due to increasing CTI with distance to the readout. In BI devices there is also a dependence on pixel column due to serial CTI. In TE mode each device is sectioned into 32x32 pixel regions, which have their unique ACIS Response Matrix Files (RMFs). Generally at this stage the differences between neighboring RMF regions is small, significant effects, however, can be noted between more distant regions resulting in differences in spectral resolving powers of up 50% from readout regions to the one farthest from readout.

Since in CC mode all rows are collapsed into one readout row, the various differences in the y- and largely the x-dependences become smeared. The result is likely a weighted average response across the entire device. However, there are two effects that mitigate the response blur in CC mode for HETG observations. The first relates to the fact that nearly all HETG observations are recorded close to the readout, i.e. within the first 512 rows. This means that the largest blur from the regions higher than row 512 get mapped into the cc-mode background only. The second relates to the fact that wider cross-dispersion PHA distributions will still be accounted for by a fairly open order sorting table. In this respect the current application of ACIS responses to the grating order extraction should have no significant effect on the HETG spectral quality. In BI devices we should encounter charge redistributions in dispersion direction in the 3x3 pixel island due to serial CTI which will be reflected in the grade distributions (see below).

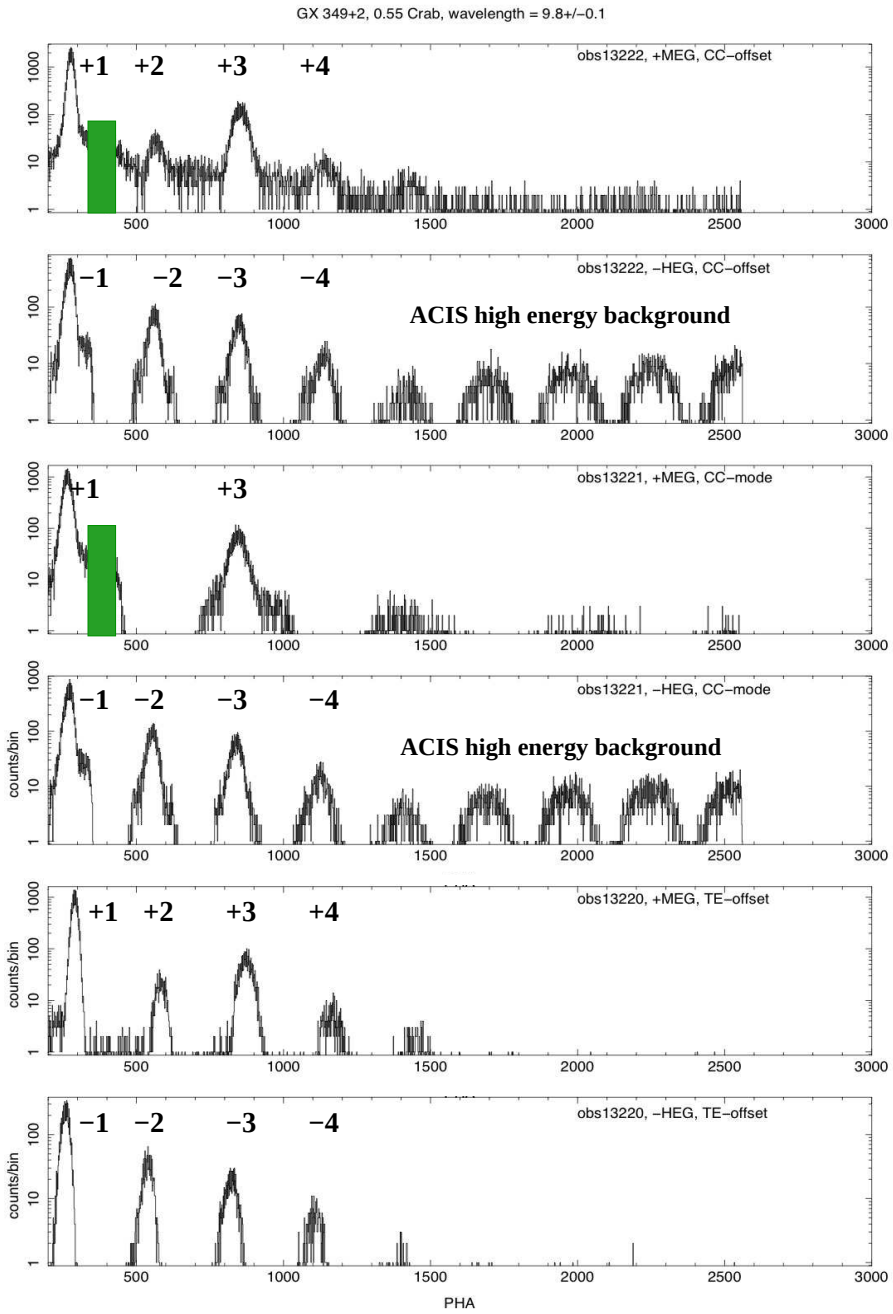

Fig. 2.— The order sorting in pha space at 9.8 Åfor in CC and TE mode in MEG +1st and HEG -1st order for different configurations as observed in GX 349+2 (see Table 1). The top two panels shows the two orders for the configuration with a Z-Sim offset of -11.3 mm in CC-mode, which puts two grating arm off the CCD array (see Figure 1, bottom). The middle two panels are the same source but with a Z-Sim offset of -6.14 mm and all grating arms are on the CCD array. The bottom panel is again the same source with a Z-Sim offset of -11.3 mm, but now in TE-mode. The numbers mark the extracted orders.

3.3. CTI Correction

Each CCD in the HETG array suffers from time-dependent CTI, which leaves charge trails in the PHA distribution altering event recognition and which allows events to drift out of the OSIP. The CTI correction in TE mode is based on measured charge trap maps for each device and node to predict charge losses across the devices and properly correct for these losses. In CC-mode charges are clocked contiuously through the Si lattice which very likely will change trap morphology and trap time scales. However, so far we did not find alternate trap maps for CC-mode that would improve corrections with respect to the ones used in TE-mode.

Figure 3 shows how the HETG events in the 1st orders line up with the ratio to its recorded energies. In a perfect world the events should scatter tightly and symmetrically around the first order sorting line marked in red. It shows that while in TE-mode observations the pipeline CTI correction aligns the resolved events very symmetrically around the order line allowing for a perfect OSIP application, the one in CC-mode does show significant deviations. In most cases these deviations are not severe enough to affect order sorting in most of the available wavelength bands. Exceptions are likely to happen in the HEG +1st orders beyond 11 Å and the MEG -1st orders beyond 16 Å. The HEG -1st and MEG +1st orders seem very well constrained in CC-mode. Main reasons for this are likely the worse CTI on S5 in case of the HEG +1st and similarly on S1 for the MEG -1st at low energies.

There are three immediate solutions available. The first simply argues to primarily use HEG -1st and MEG +1st orders only, which (see below) would also be a preferred solution for the HEG/MEG higher order background containment. The second would call for a custom OSIP, which however is due to the complex structure of the OSIP table very difficult to maintain. A third solution to improve the correction is to apply actual y-pix coordinates. The TE trap map application in CC-mode is currently very simplistic in that due to the lack of y-pix coordinates only the projected location of the of the zeroth order is used for the correction. This may be improved by one iterative step in which one actually calculates the dispersed y-pix coordinates for the entire tg_resolved HETG spectrum and applies that coordinate to a modified CTI correction. Figure 4 compares the result for an observation of GX 13+1. The top three panels are MEG, the bottom three for HEG observations. It shows that the modified CTI correction is improved with respect to the pipeline correction.

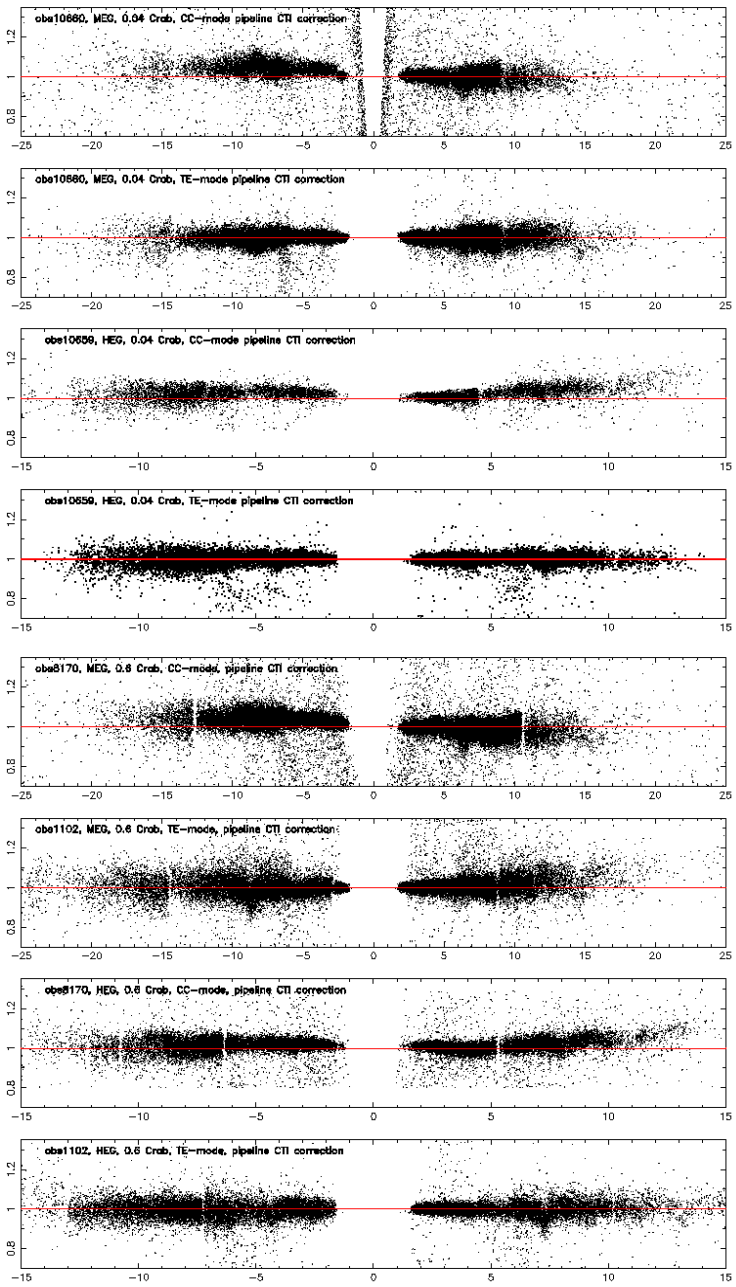

Fig. 3.— First order OSIP plots using the first 10^5 events in the tg_resolved event lists and first orders (y-scale) only. The x-scale is the *mlam* order sorted wavelength column. The top four show the pipeline corrected MEG and HEG orders for CC- and TE mode for the 35 mCrab calibration source 4U1957-115, the bottom four the same for the bright 0.6 Crab source Cyg X-2.

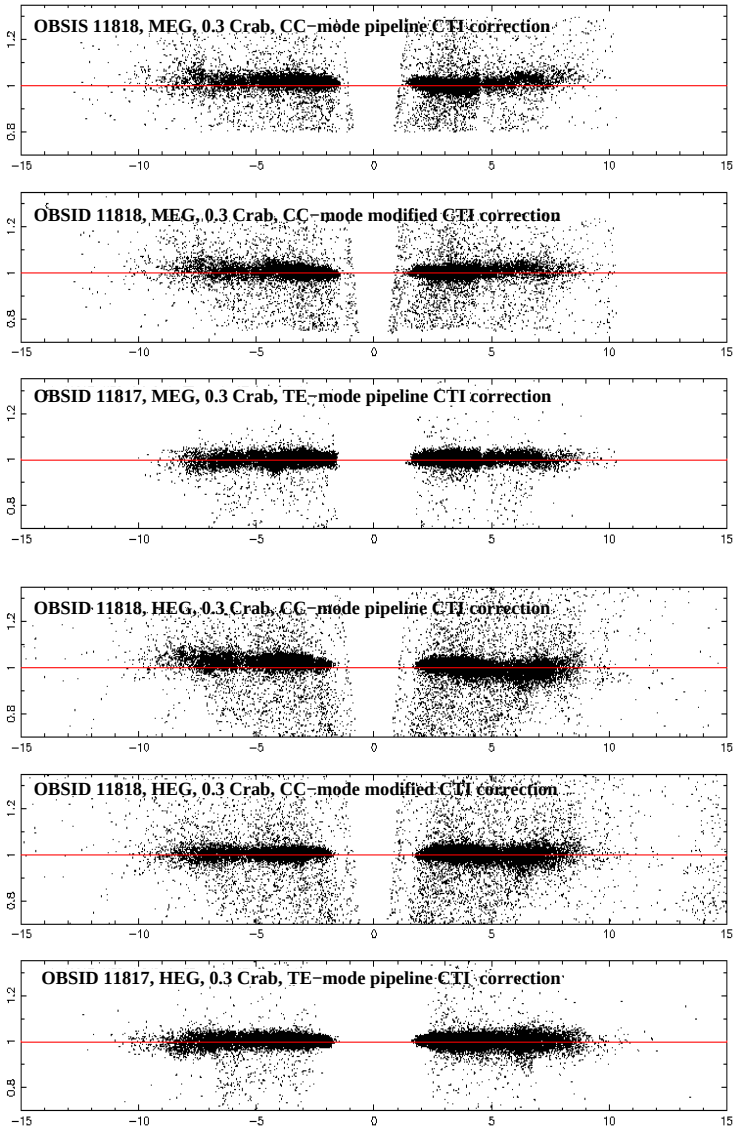

Fig. 4.— CTI correction as applied in CC mode for MEG (Top three panels) and HEG (bottom three panels) and compared to TE mode. For each grating the top shows now CTI correction, the middle shows the TE mode CTI correction of the CC mode spectra, the bottom the corresponding CTI correction applied on TE mode spectra.

3.4. Grade Sets and Distributions

One of the largest differences between TE and CC-mode are expected to come from the distribution of flight grades and how they map into the standard distribution of grades. The TE mode calibration is entirely based on the standard set of grades, which group the 255 flight grades into 7 grade categories of which three grade categories, 1, 5, and 7 are rejected and 0, 2, 3, 4, and 6 are accepted and called the standard grade set. The calibration then is always based on the sum of the these standard grades. Figure 5 (top) shows the grade distributions for a TE mode observation (OBSID 10659) for the MEG -1st order covering mostly devices S3, S2 and S1. In both device types grade 0 is the largest contributor followed by 2, 3 and 4, and 6. In S2 grades other than grades 0 only contribute to about 20% of the total, while on S1 the contributions are higher. On S3 there is a grade swap in that grade 6 becomes the dominant grade. All these effect are known and have been part of the TE mode calibration. Figure 5 (center) shows the same source (obsid 10660) observed in CC-mode. On S1, i.e. above 14 Å, the grades distribute rather similar to the TE-mode case, grades 0 and 2 seem more equally distributed. The most prominent effect we observe is on S2, where below about 10 Å grade 0 rapidly decrease and grade 2 become dominant. This is not unexpected because it means that the grade that is oriented in clocking direction becomes dominant. There are two discrete features observed: one is identified as the Si K edge in grades 3,4 and 6 similar to the TE mode case, the other one is a local drop at 8.2 Å in grades 0, 3, and 4, which seems to be compensated by an excess in grade 2 and which coincides with a CTI anomaly near the border of nodes 1 and 2 on S2. Even though there is a lot of detail in these distributions and many of these details are not well understood in TE and CC-mode, it is most important how the integrated case compares. When we integrate all standard grades over the entire bandpass, the total X-ray flux between the TE and CC-mode case agrees within 2%. This is exactly the same level of variation the source showed between the two TE mode observations which were 22 ksec apart with the CC-mode observation in between. Bin by bin variations of 0.06 Å bins between the TE and CC mode observation are limited to about 7% and appear random due to source statistics (see also Fig. 6, bottom panel).

Very bright sources are central to this CC-mode investigation and the question remains if the agreement between CC- and TE-mode also holds for very bright sources, i.e. low vs. high flux cases. Figure 5 (bottom) shows the grade distributions for S2 and parts of S1 for the case of Cyg X-2 (OBSID 8170) at 0.6 Crab. The observation had slightly different off-sets and comparable features with Figure 5 (center) appear at different wavelengths but still at similar locations on the CCD. It can be seen that the grade pattern with respect to CCD location between the low and high flux case are very similar indicating that the instrument response with respect to event detection and grade distribution is not significantly changing.

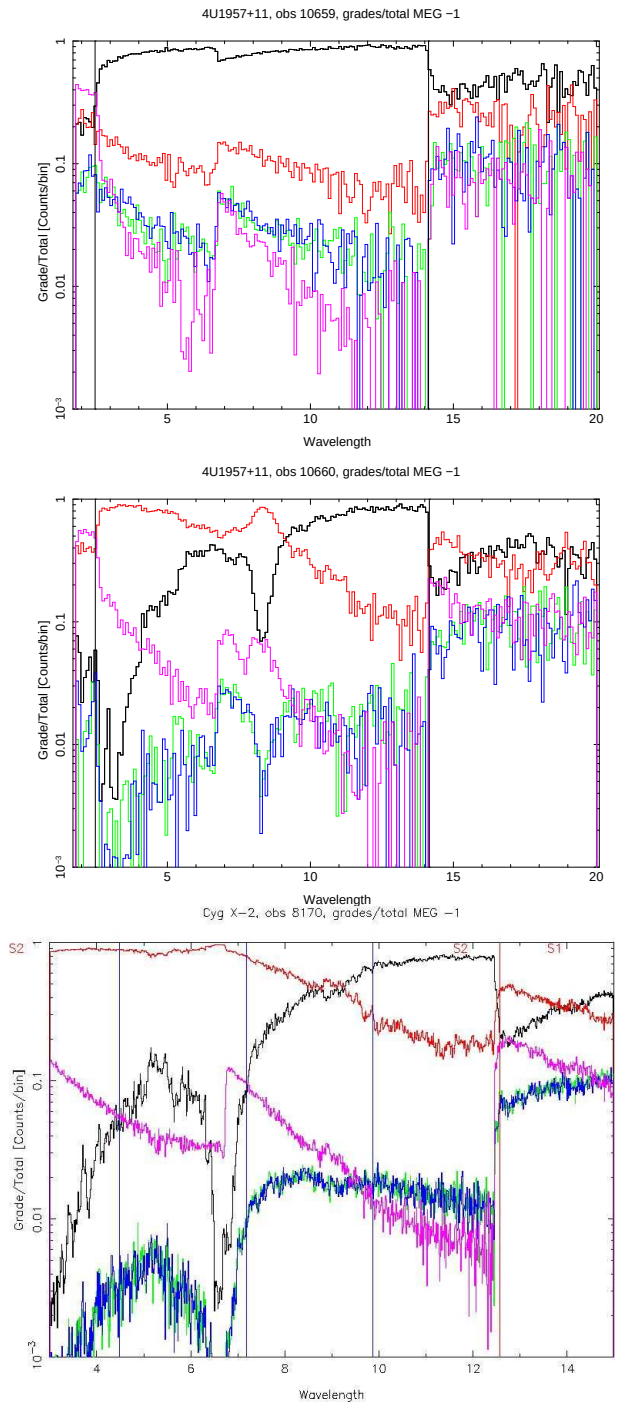

Fig. 5.— Grade distributions for 4U 1957-115 in TE (top) and CC (middle) mode at $\sim$ 35 mCrab. The bottom panel show Cyg X-2 in CC mode at 540 mCrab. The color are grade 0 (black), grade 2 (red), grade 3 (green), grade 4 (blue), and grade 6 (magenta).

We cannot make direct flux comparisons between the TE and CC-mode case because of heavy pileup in the TE-mode case and see sections below.

3.5. Faint vs. Graded Mode

Most very bright observations use onboard grade summing in order to save space in the telemetry stream. In that case only the standard grade sets 0-7 are telemetered. Generally there should not be much difference between grade and faint mode spectra and in the few cases we recorded in both, CC-faint and CC-graded, we did not observe significant differences. However, by looking outside the standard grade set into flight grades it has been noted that specifically flight grade 66, which usually is part of the rejected grade set, shows some notable enhancement and some tests revealed that specifically below 3 Å the inclusion of this flight grade may recover some lost flux up to a few percent in some cases. Since 2010 this grade and a few others are now into the telemetry stream of graded CC-mode observations.

3.6. TE vs. CC Mode Spectra

The previous sections have shown that even though there are subtle and likely differences between TE and CC mode, from the perspective of ACIS instrument calibration they all can be explained by CTI and charge trails through the clocking process. In HETG spectra these differences have practically no effect as they are largely covered by the OSIP extraction process. This can be seen in our calibration source 4U 1957-115 (Fig. 6, where we have successive TE and CC-mode spectral coverage and no intrinsic spectral variation between these observations. In general the CC-mode extractions of the four grating arms, MEG -1st order (black), MEG +1st order (red), HEG -1st order (green), HEG +1st order (blue), overlap well both in CC- and TE-mode. The match can be checked best in the bottom panel which shows the corresponding ratio between the TE- and CC-mode spectra. Towards the soft end there is a slight difference of a few percent between the MEG and HEG, which is explained by a higher order overlap and which is addressed in Sect. *High Order Background* below.

The fact, however, that there are observed differences and problems in HETG CC-mode spectra is demonstrated in Figures 7 and Figures 8. These are HETG spectra of bright X-ray binaries for a variety of fluxes, spectral shapes and absorption. While some cases show quite dramatic effects, such as in Cyg X-2, Cyg X-1, or GX 339-4, some others such as 4U 1630-47 are hardly or not affected at all. Most sources in these two figures have fluxes above 200

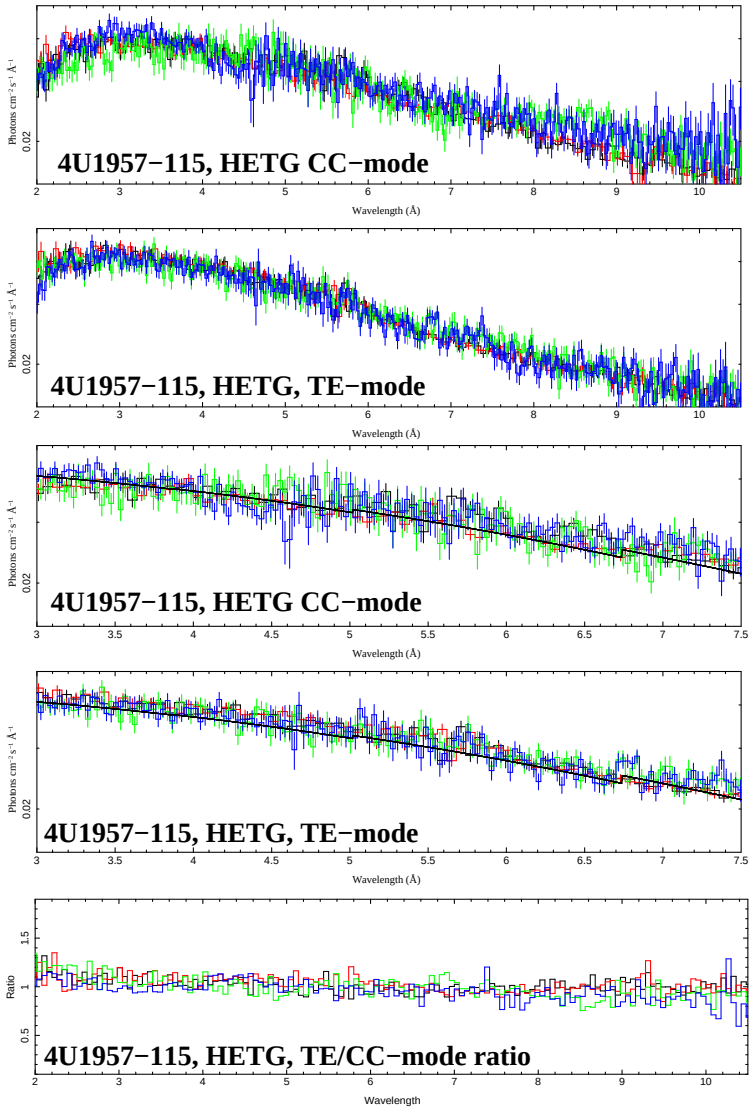

Fig. 6.— Comparison of HETG spectra for 4U 1957-115 in TE and CC mode at $\sim$ 35 mCrab. The top two panels shows the the 2 - 10.5 Å bandpass, the middle two panels a blowup of the critical 3 - 7.5 Å bandpass. The bottom panel shows the ratio of TE over CC mode spectra for the four 1st orders. MEG -1st is black, MEG +1st is red, HEG -1st is green, and HEG +1st is blue.

mCrab.

In the following we describe effects specifically affecting HETG spectra and possible fixes.

4. Why is CC mode different for HETG spectra

There is a major difference between TE and CC mode HETG spectra in the way they are recorded. While in TE mode the dispersive imaging properties are completely preserved, in CC mode one dimension is collapsed and this has severe consequences, specifically for sources with X-ray columns larger than 10^{21} cm^{-2}. In essence most CC-mode effects strongly depend on the source image and the incident source spectrum and are therefore predominantely science isseus.

We have identified three major effects that can alter the extracted HETG spectra in CC-mode with respect to TE-mode:

- *Additional extended source dispersions:* this effect is primarily caused by extended source emissions which also disperse and by the clocking process merge differently into the four HETG spectral arms. In bright absorbed X-ray binaries this is a significant scattering halo in the source image. Another feature, however at a much lesser scale, originates from dispersion of a significant scattering tail of the psf which in some cases can affect the cross-dispersion flux normalization.

- *High order backgound:* this affects HEG 1st order spectra from a direct overlap with MEG 2nd order spectra.

- *CC-mode (soft) background*: in CC-mode all 1024 rows of a device get clocked into each other enhancing any charge background that is not visible in TE mode by several orders of magnitude but becomes significant in bright sources.

5. The Scattering Halo in CC-mode

The primary effect we identified and which can alter dipersed source spectra in HETG in various ways is the apparent X-ray source scattering halo present in brighter and more absorbed sources. Figure 9 shows five examples of HETG images including the zero order image. The bottom panel shows our calibration source 4U 1957-115, which at a flux of 35 mCrab and an absorption column of about 1.5×10^{21} cm^{-2}. Even though the X-ray source is

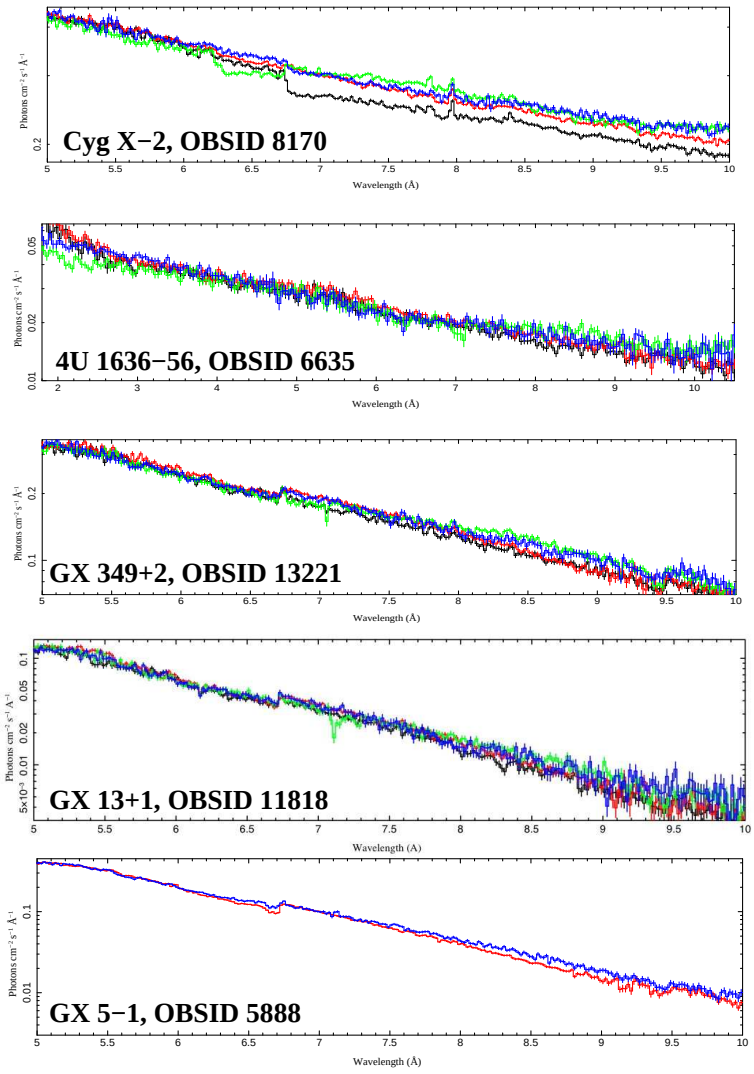

Fig. 7.— Various CC-mode HETG spectra for for bright LMXBs above 50 mCrab and various spectral shapes. MEG -1st is black, MEG +1st is red, HEG -1st is green, and HEG +1st is blue.

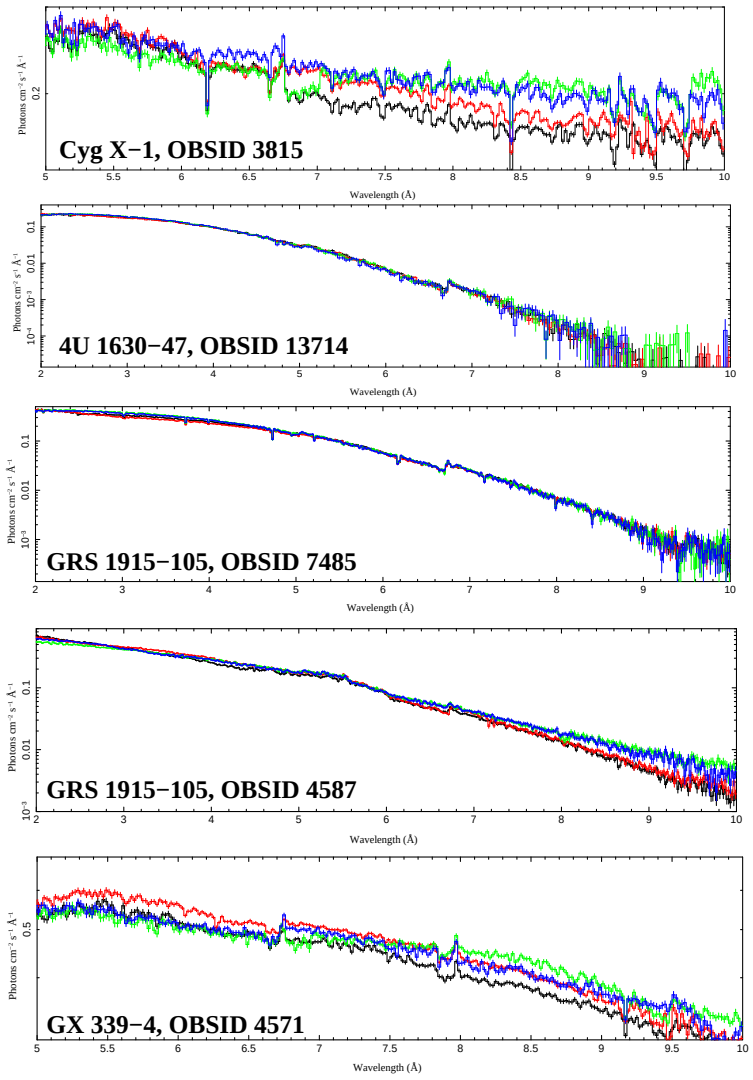

Fig. 8.— Same as Figure 7 but for bright BH sources above 200 mCrab

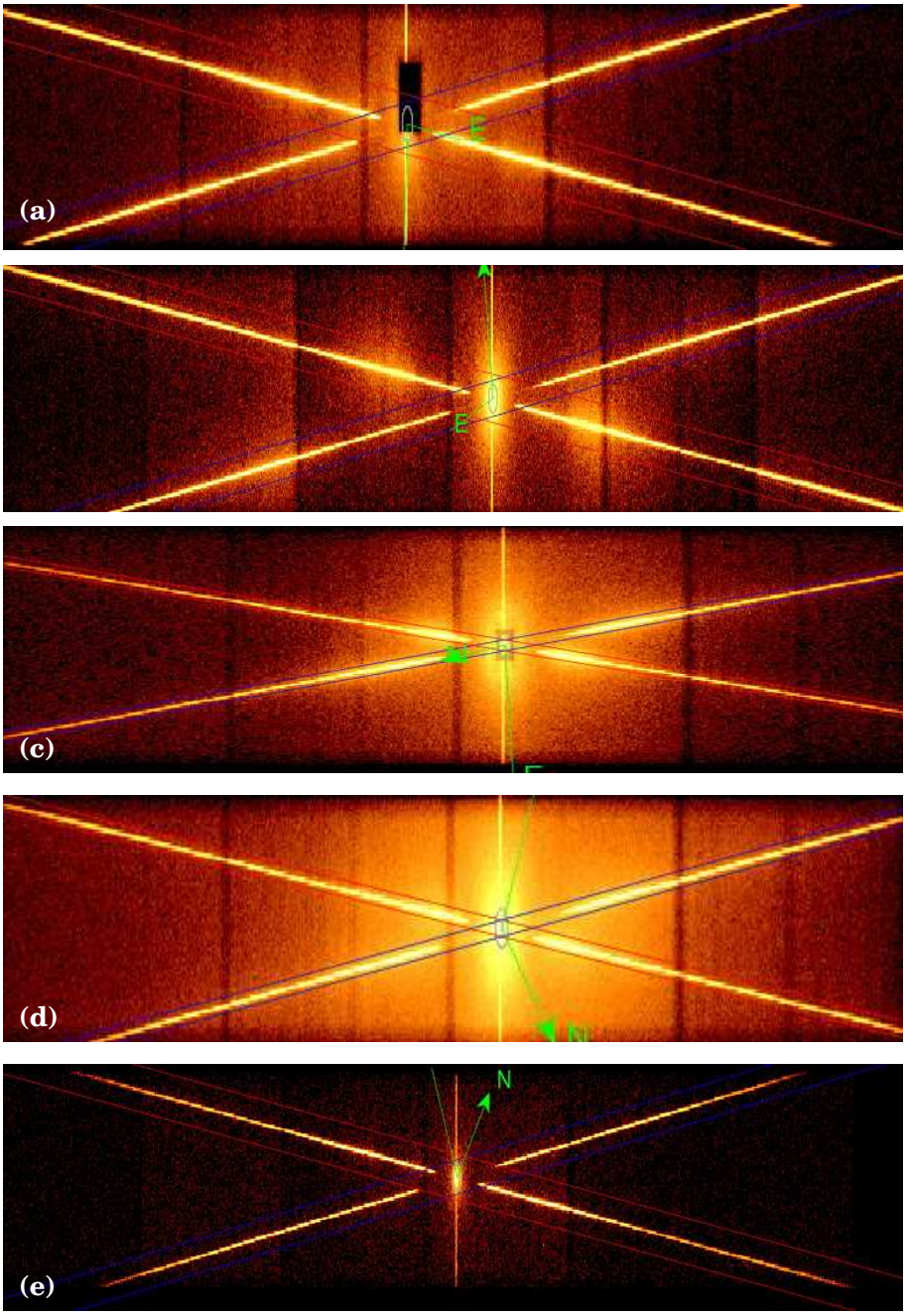

Fig. 9.— Five cases of X-ray scattering halos and its dispersion observed with HETG in TE mode. The colored regions indicate the extraction regions for MEG (red) and HEG (blue) spectra. The green arrow marks the orientation towards north in the system. The central oval is the zero order extraction region. **(a)** The HETG extraction regions and arrays of Cyg X-2 ($\sim$ 450 mCrab) is moderately absorbed with about 3×10^{21} cm^{-2} column density in the line of sight. **(b)** The same for Cyg X-1 ($\sim$ 650 mCrab) at 8×10^{21} cm^{-2}, **(c)** for 4U 1630-47 ($\sim$ 200 mCrab) at 1×10^{23} cm^{-2}, **(d)** GRS 1915+105 ($\sim$ 400 mCrab) at 5×10^{21} cm^{-2}. **(e)** is the calibration source 4U 1957-115 ($\sim$ 35 mCrab) at 1×10^{21} cm^{-2},

relatively soft, the source is faint enough to not produce a significant CC-mode background and has low enough absorption to not produce a significant dipersed overlapping scattering halo. Consequently HETG spectral arms agree well in the specified bandpass in TE and CC-mode as shown in Figure 6.

This appearance changes dramatically in sources with higher fluxes and absorptions. Panels a - d in Figure 9 shows four examples. As dramatic as these pictures appear, however, not all what is seen as bright diffuse emissions actually has an effect of the dispersed spectra of the point source because of the order sorting in PHA space, which acts as a filter. An example is a comparison of panels c and d, which has corresponding HETG spectra in Figure 8, OBSID 13714 and 4587, respectively. While the spectra in OBSID 13714 show little altercations, OBSID 4587 does, even though the sources are similarly bright and absorbed. However, the source spectrum in OBSID 13714 is very hard, it drops over three orders of magnitudes in the specified bandpass, while the one in OBSID 4587 drops less than two orders of magnitudes. In sources such as in Cyg X-2, Cyg X-1, GX 339-4 (see Figures 7 and 8) spectra are very flat and soft and even though absorption does not appear as high, its dispersed halo spectra produce most visible distortions. How sensitive the shape of the source spectrum is for this issue can be seen in the two shown spectra of GRS 1915-105 (see Figure 8). While in OBSID 7485 the spectrum drops again rapidly allowing for the OSIP PHA window to be a much more effective filter and thus CC-mode obstruction effects are comparatively small, in OBSID 4587 the spectrum of the same source is now much flatter and obstruction effects including MEG higher order overlaps (see below) have a much more significant effect on the measured spectra.

Figure 10 attempts to illustrate the effect of a dispersed scattering halo plus other effects (see below) on the extracted source spectrum. The spectrum of the scattering halo is usually soft and affects spectra below about 3 keV. However the exact shape of the spectrum is unknown and part of extensive science investigations. Spectra can be affected above about 3 keV depending how much the Si K and maybe even the S K edges are compromised. The top panel simply illustrates how the source image consisting of a point source and a scattering halo disperses in MEG and HEG and which CCDs are primarily accupied. The middle two panels then show how the actual source spectrum gets distorted by a smeared dispersed halo spectrum. The smear in the halo spectrum comes from the fact that the gratings in HETG are inclined with respect to the readout direction. A large fraction of halo event overlap with the OSIP extraction window and add to the actual source spectrum. Together with CC-mode backgrounds, a different treatment of the Si K edge in FI and BI devices, and MEG higher order overlaps in the HEG, the actual source spectrum gets distorted in different ways for each spectral grating arm. This is illustrated in the bottom panel of Figure 10 which show all modified spectral arms with respect to the actual source spectrum.

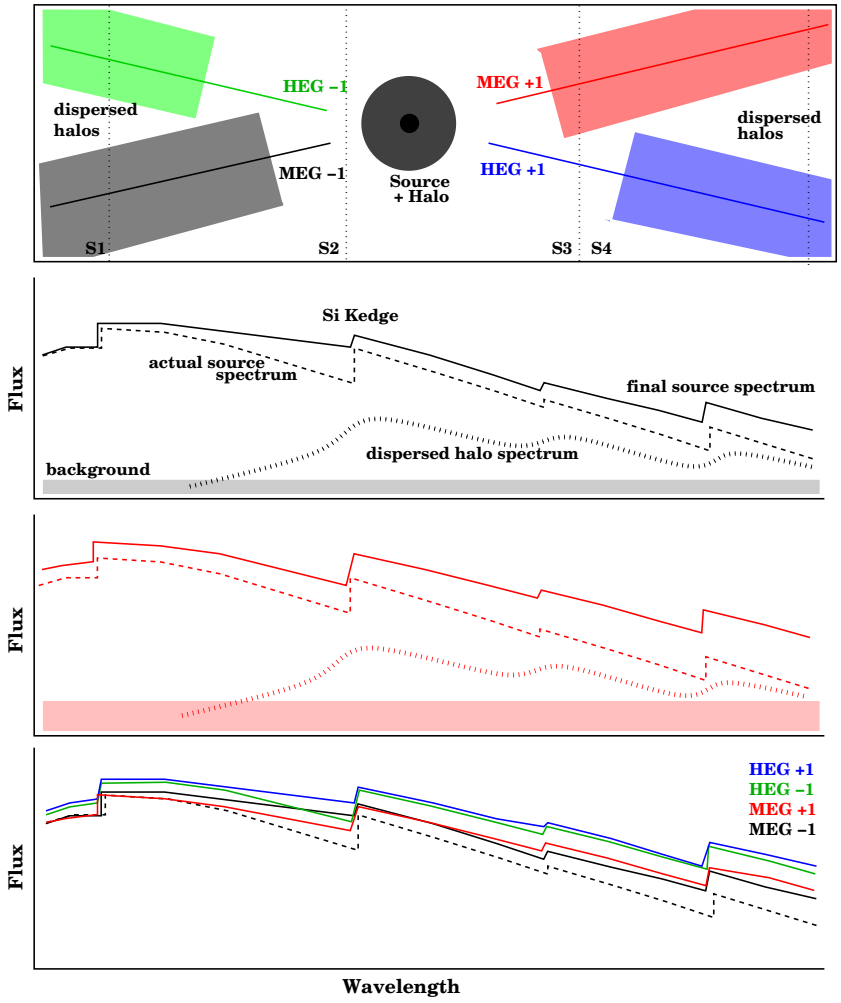

Fig. 10.— A sketch illustrating the effect of various spectral obstructions to the dispersed source spectrum due to collapsed dispersed images in CC-mode. At the foremost a spectral overlap at soft X-rays due to a smeared dispersed halo spectrum. The top panel illustrates the image effect, the middle two panels the effects on the MEG -1st (black) and MEG +1st (red) spectra. While the soft halo spectrum is likely very similar, there are different CC-mode backgrounds and Si K edge modifications. In the MEG +1st order the Si K is least affected since it falls on a BI (S3) device. The bottom spectrum shows all four HETG spectral arms on top of each other with respect to the actual source spectrum (dashed line). Here the HEG spectra, HEG -1st (green) and HEG +1st (blue) also appear syatematically higher in the soft range because of MEG higher order overlaps. The HEG -1st spectrum also is less modified iat the Si K edge because it falls on a BI (S1) device

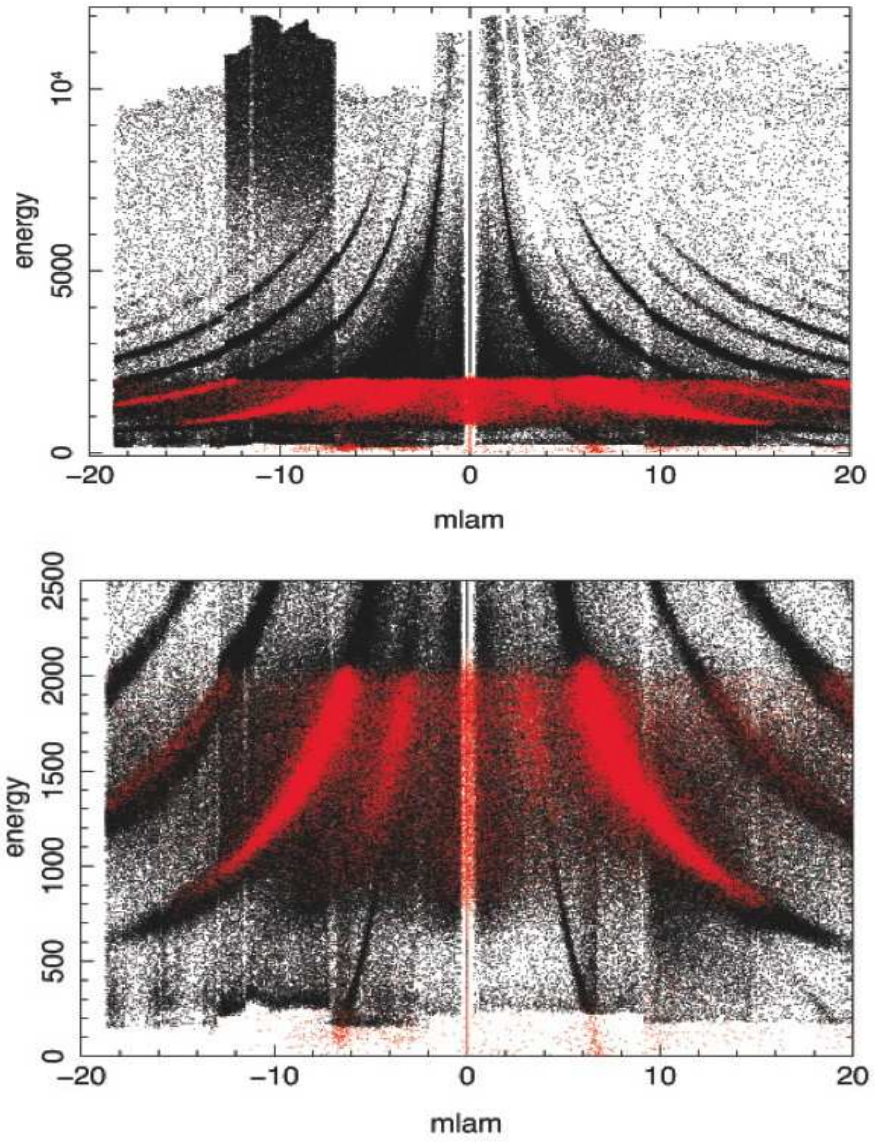

Fig. 11.— MARX simulation for the case of Cyg X-1 in a configuration where one MEG and one HEG spectral arm were kept off the CCD array. The black points are from a typical Cyg X-1 source spectrum, the red points are from a halo spectrum below 2 kev. The to panel show the resolved events for HEG minus (left side) and MEG plus (right side) orders for the full available energy scale. The bottom panel is limited to 2.5 keV. In the simulated case to halo sppectrum full overlaps with the HEG -1st and MEG +1st orders creating the mismatches of the spectra such as observed in Figure 8 top panel.

Such an extended halo dispersion can be modeled using MARX. Figure 11 shows such an attempt for Cyg X-1 indicating the order overlap of point source and halo. The effects of the dispersed scattering halo in general depends significantly on the shape of the source spectrum as well as the spectrum of the scattering halo itself. Depending on both shapes the actual source spectrum in the HETG orders are either insignificantly affected or grossly distorted. Should the latter be the case, the determination of the actual source spectrum in HETG CC-mode spectra requires detailed modeling of the interstellar scattering halo spectrum The observer then needs to model interstellar X-ray scattering which is a foremost consequence of the line of sight composition, density, and abundance of the interstellar medium and thus a difficult science project.

5.1. The Si K and other edges

The illustration in Figure 11 also indicates that photoelectric absorption edges are also affected by the halo dispersion. The scattering halo spectrum also has photoelectric absorption edges naturally from the same line of sight. However, as also indicated, because of the slight inclination of the gratings toward the readout, these edge have a slight smear as well as have some different optical depth pending of the scattering medium. This will affect at least the measured optical depth in the edges of the actual source spectrum and likely lead to a decrease in the measured value for all the edges that appear in the halo spectrum. Which ones at the end appear and at which depth has to be modeled. Figure 12 shows a MARX simulation (courtesy of J. Lee et al.) for GRS 1915+105 and Si K. In the case of a pure point simulation the outcome of CC- and TE-mode should be the same, not accounting for the slight smear effect. However, once the simulation adds a additional extended emissions, the CC-mode case records a significantly lower optical depth. In the case of GRS 1915+105 the effect is expected to be extreme because of the expected intrinsic dusty environment of the X-ray source and accounts for an almost 40% loss in optical depth. We estimated from Si K edges of many other X-ray binaries using TE versus CC-mode data that effects amount to between 5 and 20%.

5.2. Si K edge Overcorrection in FI Devices

The Si K edge in the HETG CCD array is a specifically complex issue because while the BI device has its SiO_2 gate structure removed and is illuminated from the backside, its quantum efficiency function does not feature intrinsic Si K absorption. This is different in front illuminated devices, where X-rays have to penetrate a substantial layer of SiO_2.

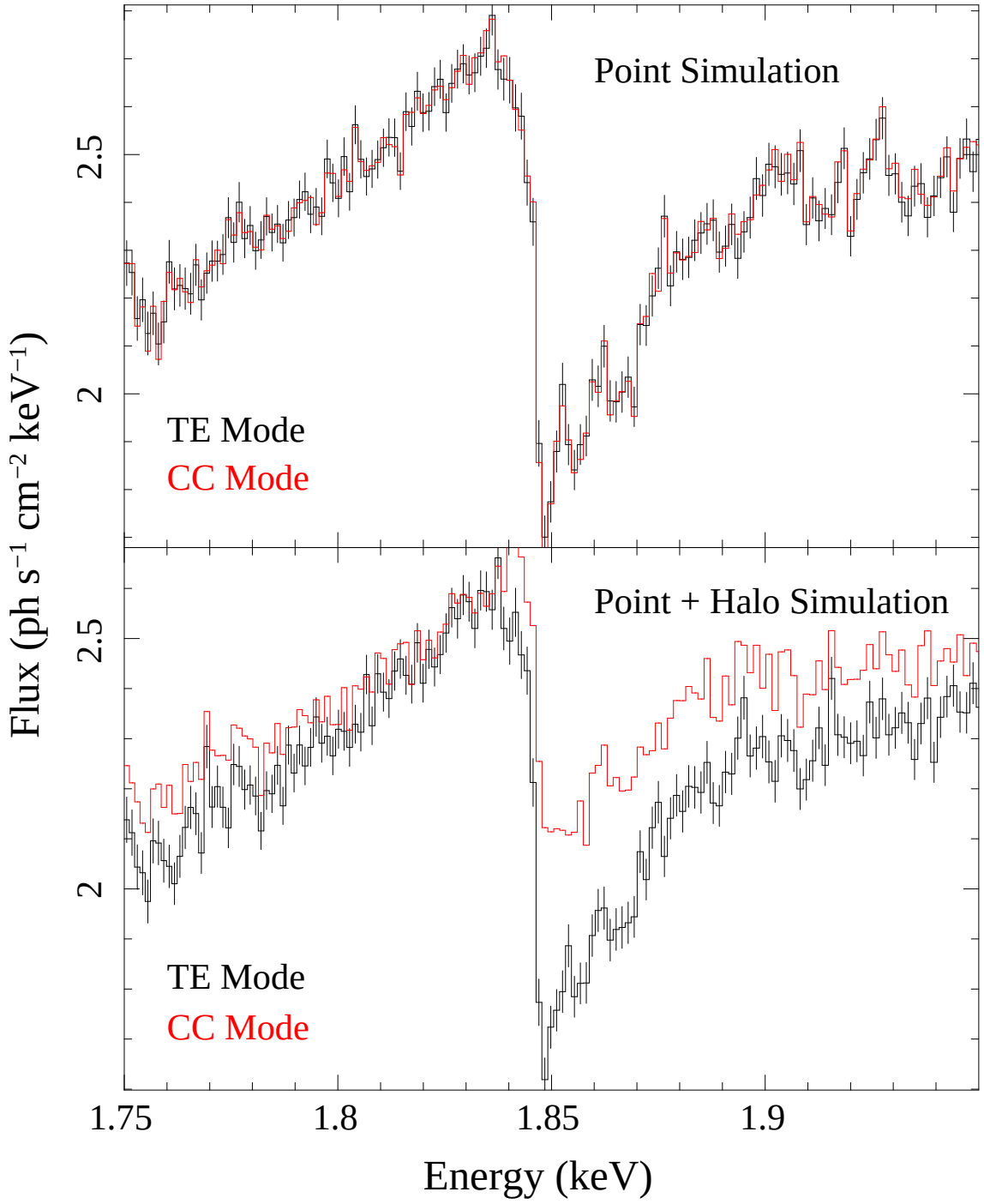

Fig. 12.— Marx simulation of a Si K edge for the case of GRS 1915+105. The top figure shows the case where the X-ray source is a single Chandra point source dispersing the standard Chandra point spread function (psf), the bottom figure adds flat scattering halo to the pdf which in the case of CC mode gets collapsed into the extracted HETG spectrum.

Figures 13 and 15 show how this manifests itself in CC-mode data around the Si K edge for the cases of low and high absorption columns iin the bright binaries Cyg X-2 and 4U 1728-34. While in the case of Cyg X-2, which has a low column, the Si K edge in the MEG +1 and HEG -1 orders is clearly visible and its optical depths are of the order of its expected value, in the MEG -1 and HEG +1 orders it either does not exist or even an excess appears. The reason for this behavior lies in the nature of the CCD devices in the array. The previous cases both fall on BI devices, the latter cases are on FI devices. Since BI devices do not need an instrumental Si K correction, its absorption column is high enough and the source is bright enough to produce a measurable edge at Si K, only affected by the extended halo dispersion. The FI the edge is also affected by the halo dispersion; however while the halo corrected part gets blurred and thus the applied correction is slightly off, the source part still gets corrected properly. This combination can lead to an imprint of the instrument correction function as observed in Figure 14 in the left panel, where the residuals clearly indicate the SiO_2 transmission features in the data. This effect is only visible as such where the source Si K edge optical depth is low enough to be statistically comparable to the halo fill rate Such sources include Cyg X-2, 4U 1828-30, and GX 339-4.

In sources with high Si K depth from the absorption column this effect appears less subtle in that one observes that edge depths on BI devices to be larger and much closer to the expected values, while in FI devices the edges are more blurred and appear with less optical depths. Independent of whether the absorbing column is low or high, the effect again has to be modelled in the context of an absorption scattering background and is thus part of the science analysis.

5.3. The 5.44 Å Effect

While most of the additional dispersive additions we observe in HETG CC-mode spectra are of broadband nature, there is one local feature that appears in almost all spectra. The feature is a broad but localized excess centered around about 5.4 Å (2.4 keV). It appears like broad line emission. The feature appears independent of the CCD array morphology and is likely again related to extended dispersion features. Evidence for that is that it appears in MEG and HEG at the same location not only in the 1st orders but also in higher order spctra. We currently have no plausible explanations for the effect and we are trying to reproduce the feature through MARX simulations. Due to its dispersive nature, we stongly suspect some connection with again the halo obstruction effect.

6. CC-Mode Backgrounds

There are two background components to consider in CC-mode observations using the HETG. First there is a clocking background which essentially is the standard TE-mode CCD backgound multiplied by the number of clocking rows, i.e. 1024 pixels. The other components is related to HEG spectra and stems from a higher MEG order spectral overlap.

6.1. Clocking Background

This background component arises naturally based on the existing CCD background. In TE-mode observations the background in each pixel is very low and negligible for most HETG spectra. It becomes important in CC-mode as it gets amplified by about a factor 10^3 during the clocking process. The backgound rates are chip dependent and thus the impact on the four grating arms will be different on ACIS S-array. This accounts for some of the divergence observed in MEG and HEG +/- orders in Figures 7 and 8. The rates are also slightly energy dependent and some of the rates per second and CCD are listed in every years Proposers Observatory Guide.

The largest differences in rates are between BI and FI devices and this makes the background contribution discontinuous in HETG dispersion direction. In order to model this backgound component one thus has to include the aspect solution which should be done with MARX in sync with the halo modeling. Commonly one can also try to extract this backgound also in the PHA order sorting window, which is described in "Future Observation Guidelines" below. In most cases it might be sufficient to account for the contribution at low energies (high wavelengths) only since here most spectra become fainter and background is statistically more signaificant. In that case one might simply subtract a flat rate corresponding to the FI/BI rates in each spectral arm. Extraction of this background can be done by selecting pulse heights in between orders as indicated in Fig 2 (green box) for the MEG +1 first orders.

6.2. High Order Background

The TE-mode order sorting in HETG observations relies on spatial and CCD spectral separations of MEG and HEG and their higher orders. MEG and HEG spectra are spatially separated and once extracted the CCD PHA space separates the higher order very effectively. In CC-mode this is no longer the case as here MEG and HEG are no longer spatially separated and their orders can overlap in CCD PHA space.

This can be seen in Figure 2. In standard CC-mode observations the OSIP blanks out the MEG even orders during extraction, however physically the even order counts are still recorded. This cannot be changed. The means that counts from mostly the the MEG 2nd orders will overlap into the HEG 1st order, Other overlaps are unlikely in PHA space due to the dispersive nature of the gratings. The MEG second order efficiencies are about 5In order to account for this overlap HEG 1st order spectra should then have multiple responses assigned, HEG 1st order and MEG 2nd plus 3rd order.

7. Future Observation Guidelines

Observations of very bright X-ray sources with the HETG in CC mode in most cases require careful choices of configurations and modes as well as background subtractions and spectral modeling. The following summarizes a few suggestion what the observer and analyst can do in order to successfully extract and model the X-ray source spectrum in the HETG gratings.

7.1. Configurations

There are various configurations one can choose to mitigate either pileup in TE mode or background and imaging effects in CC mode. While the choice of subarrays in TE proves to be an effective tool in most cases, such a choice is not available in CC mode. Two configurations are being considered. The first is the standard configuration with all four grating arms on the CCD array. In this case the zero order should be moved as closely as possible towards the readout of the CCD to optimize order sorting and allow for sufficient PHA space in between orders for efficient background extraction (see below). The second configuration puts two grating arms off the CCD array, i.e. moves the zeroth order right next to the first readout row. This is shown at the bottom of Fig. 1. Even though this comes at the expense of about half of the maximum exposure such a configuration has several advantages.

The first advantage is that it eliminates the higher order background in the HEG as the corresponding MEG orders are off the CCD array. It also eases the standard background extraction as HETG orders remain well separated at all times. It also has grave advantages with respect to the modeling of the effect of the scattering halo and the dispersion of the psf scattering wings. The main advantage is that because only parts of the zero order image components disperse, that edges in the spectra are much less affected and the spectra in

orders are much better in agreement. Last but not least in this configuration both Si K edges can be put onto BI devices. For this a Y-offset of about +1 arcmin needs to be applied from the nominal aimpoint. In general this configuration will greatly ease the modeling effort.

7.2. Background/Halo Extraction

There are several ways to extract the standard CCD background. Basis for the extraction is the order sorting in pha space as shown in Fig. 2. The background is extracted from the speces in between the orders as indicated by the green regions for the case of the MEG +1st order. To date there is no specific tool available to do the extraction and currently one has top do it manually.

However there is a *vwhere* tool in the testing phase for the next *ISIS* release. The tool *bsub* allows to extract backgrounds in between orders on an interactive basis. Key here is to efficiently exclude all source photons in the the OSIP extraction and normalize the remainder to the excluded source area. An example of such an extraction is shown in Fig. 17. The blue polygon contour in the left panels is the chosen envelope for all the source counts within the OSIP extraction window. The count spectra in the left panel are the corresponding background extractions. In the case of the 4U 1957+115 the background contributes up to about 5% to the total spectrum. The backgounds in Fig. 17 appear to have only a slight dependence on wavelength and some dependence on CCD location. The background appears continuous because of the telesope dither. The background levels are higher than predicted from the POG standard CCD background values once normalized to CC-mode and the chosen extraction regions which is expected due to some contributions from faint source and halo scattering events.

The application of this tool is limited as it does not account for the direct effects of all additional dispersive components on the source spectra. It can be useful in cases where additional dispersive components are minimal or when the suggested configuration with two grating are off the array is used. Fig. 18 shows an example for such an analysis for the case of Cyg X-1 in an CC-mode observation with this configuration. Here MEG +1st and HEG -1st orders are available and after correcting for the extracted background both are in quite reasonable agreement. However, there is still a residual systematic effect of the edge altercations to be considered in the final analysis.

7.3. Modeling

In most cases all additional spectral components that are present in CC-mode HETG spectra need to be modeled during the science analysis. This also includes the standard CC-mode background for the simple reason that it is merged into the other dispersive imaging components. At this point there is yet no example available but one will be provided at a later stage. For now the observer should utilized *MARX* to model the dispersion of the source scattering halo, apply the full energy dependent point spread function with its dispersion of the core plus scattering wing, and the distribution of the standard CCD background.

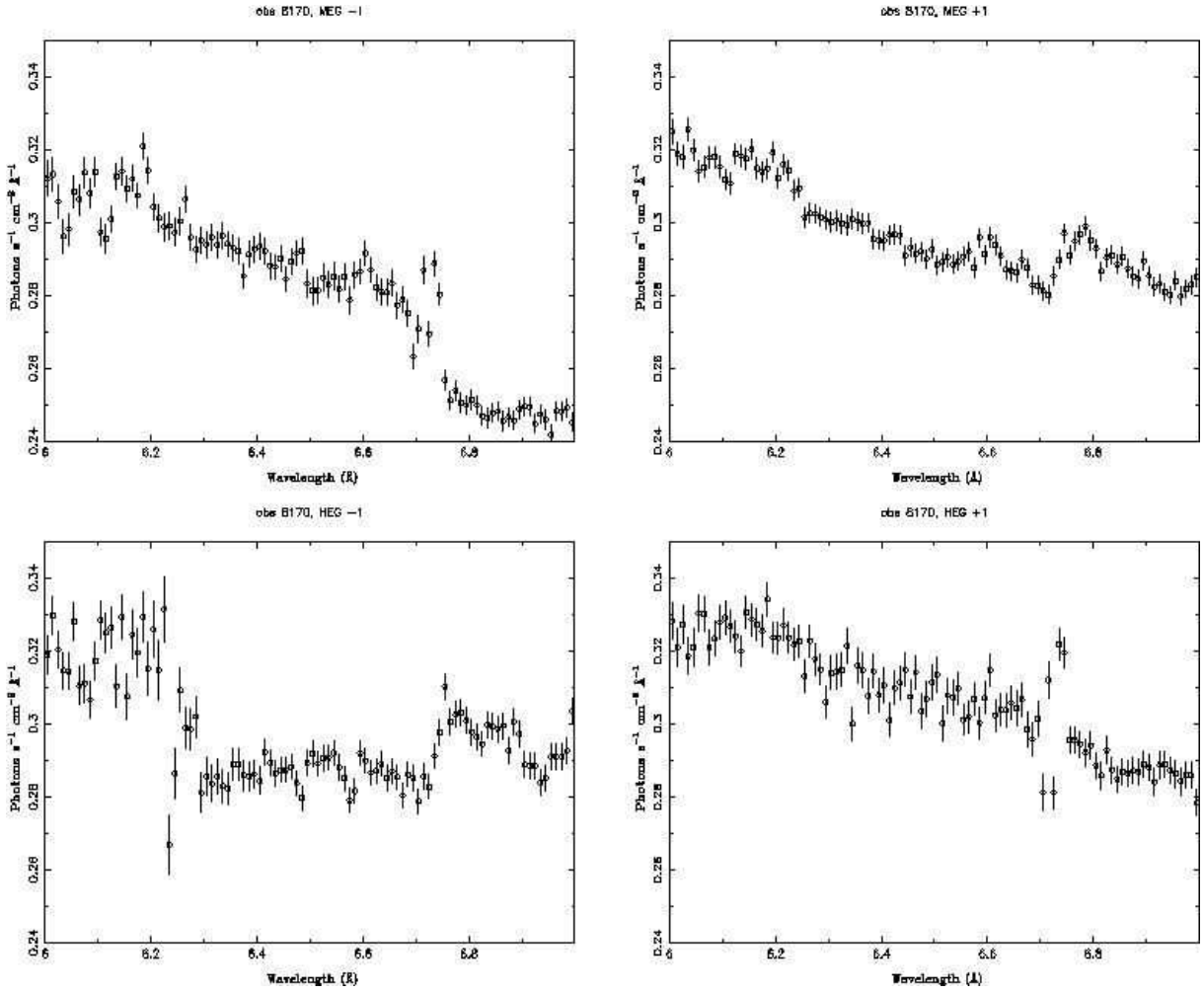

Fig. 13.— Appearance of the Si K edge in all four spectral arms of the ± 1st order in MEG (top panels) and HEG (bottom panels) for Cyg X-2 in CC mode, which has an absorption column of around 3×10^{21} cm^{-2}.

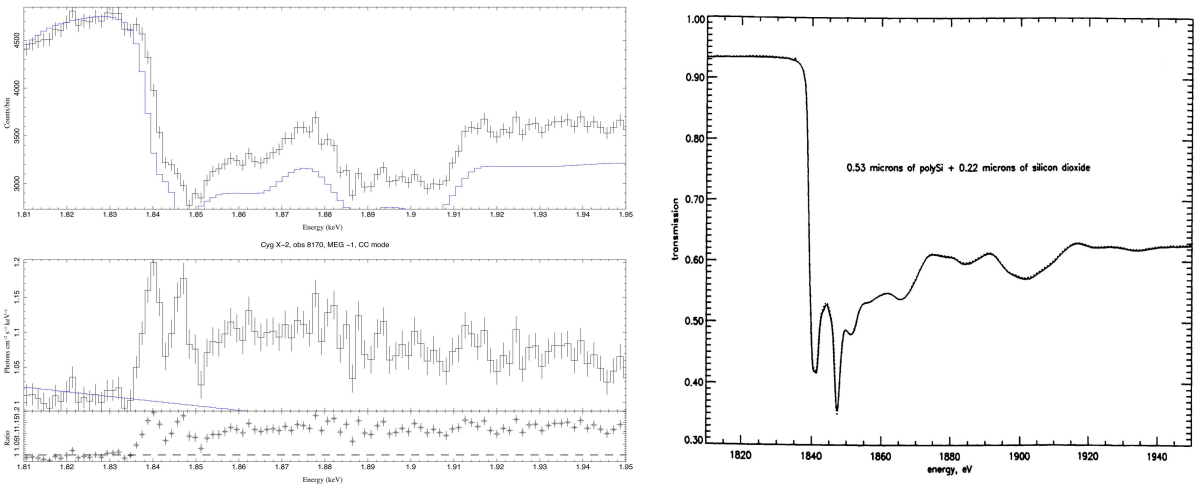

Fig. 14.— **Left:** The Si K edge in Cyg X-2 on a FI device. Due to the edge fill of the scatting background the Si K instrument correction gets imprinted into the residuals. **Right:** The SiO_2 transmission function measured for FI devices in ground calibration.

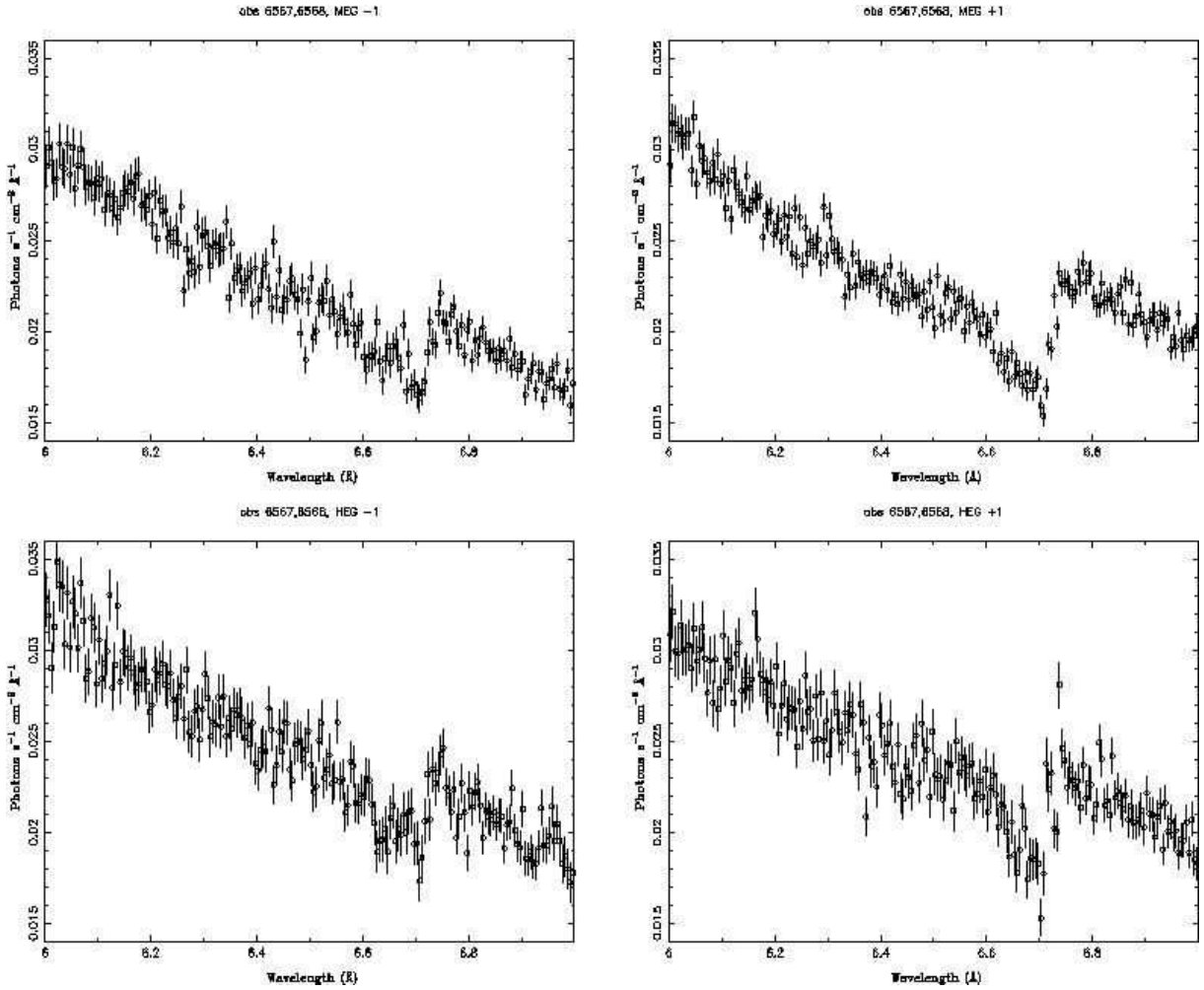

Fig. 15.— Appearance of the Si K edge in all four spectral arms of the ± 1st order in MEG (top panels) and HEG for 4U 1728-34 (bottom panels) in CC mode, which has an absorption column of around 2.5×10^{22} cm^{-2}.

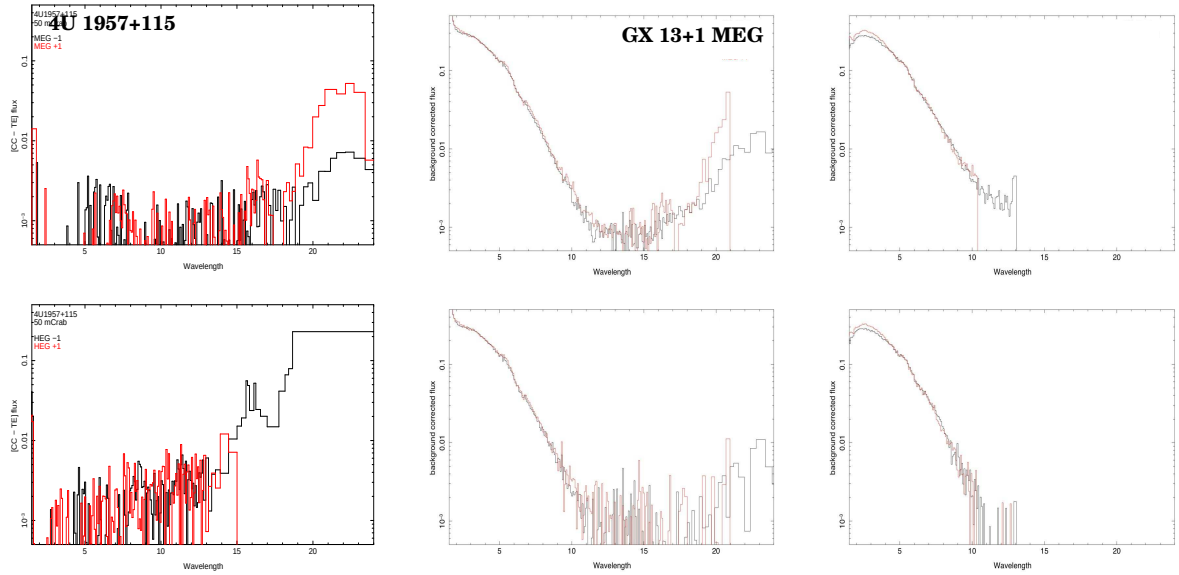

Fig. 16.— Background correction from data. **Left:** Difference spectra for 4U 1957+115 between TE and CC mode observations. These difference spectra account for all the backgrounds between TE and CC-mode. **Middle:** Application of these background spectra to GX 13+1 for the MEG +1st (red) and -1st (black) orders. The top panel is the uncorrected data, the bottom with the background data applies. **Right:** Same for HEG -1st (red) and +1st (black) orders.

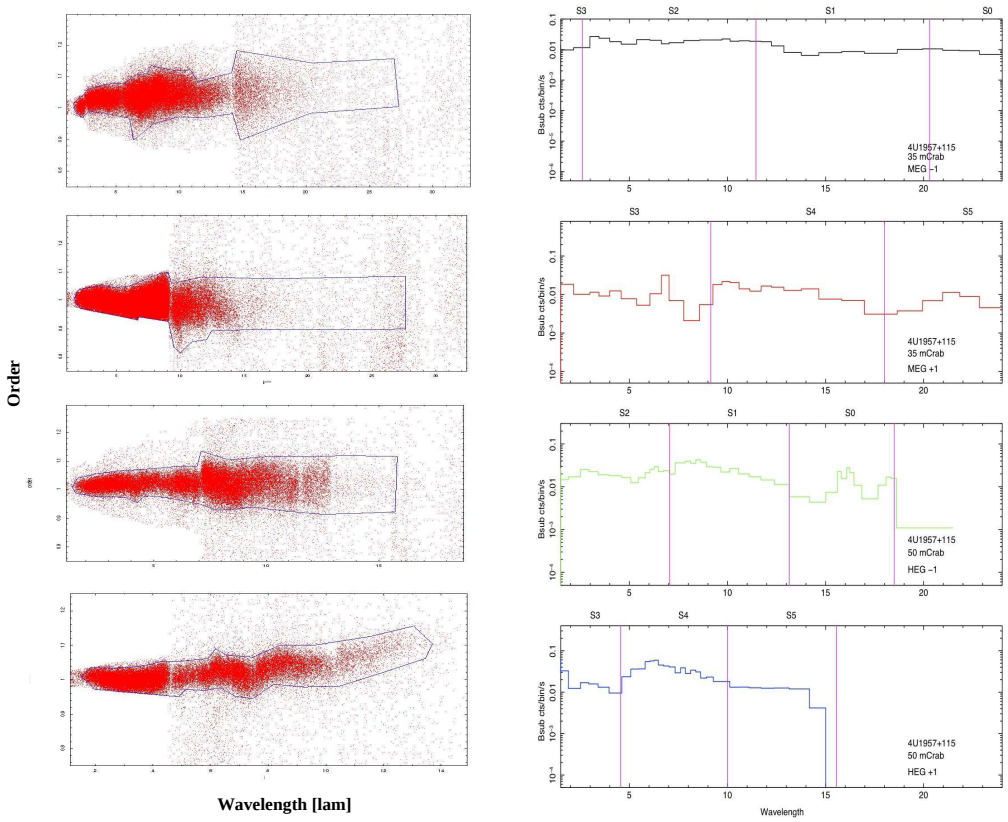

Fig. 17.— Background extraction from data. **Left:** Extraction regions using the order sorting plot for the 4U 1957+115 CC-mode observation (OBSID 10660), MEG -1st, +1st, HEG -1st, +1st from top to bottom. **Right:** The corresponding extracted background spectra in the same order. The CCD boundaries are approximate as they dither smeared, which also makes the background spectra look fairly continuous.

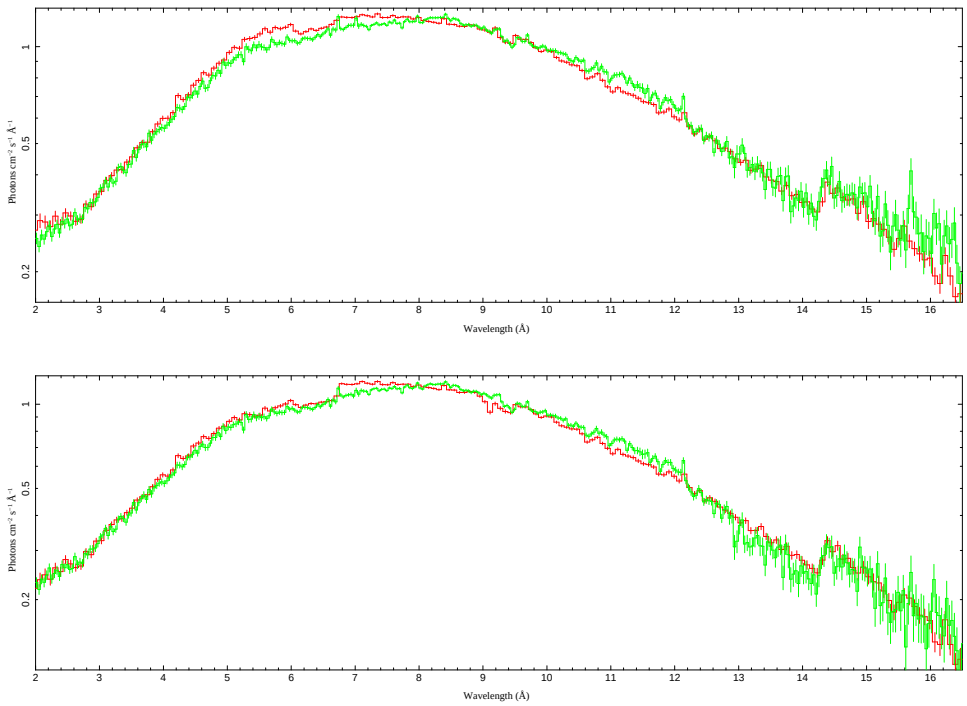

Fig. 18.— Background/halo subtraction from Cyg X-1 data in the suggested CC-mode configuration placing two grating arms off the CCD array (place holder)